Ocean Engineering 270 (2023) 113613

Contents lists available at ScienceDirect

Ocean Engineering

journal homepage: www.elsevier.com/locate/oceaneng

Wave interaction with a concentric bottom-mounted cylinder system with dual porous ring plates

MoHan Zhang [a,d], Xiang Wang [b], GuangYuan Wang [c,*], Jin Wang [e], PengYuan Zhao [e]

[a] Key Laboratory for Mechanics in Fluid Solid Coupling Systems, Institute of Mechanics, Chinese Academy of Sciences, Beijing, 100190, China
[b] College of Shipbuilding Engineering, Harbin Engineering University, Harbin, 150001, China
[c] National Engineering Research Center of Port Hydraulic Construction Technology, Tianjin Research Institute for Water Transport Engineering, M.O.T., Tianjin, 300000, China
[d] School of Engineering Science, University of Chinese Academy of Sciences, Beijing, 100049, China
[e] China Ship Development and Design Center, Wuhan, 430000, China

ARTICLE INFO

Keywords:
Wave diffraction
Concentric cylinders
Porous ring plates
Hydrodynamic force
Free surface elevation

ABSTRACT

The interaction between linear surface waves and a concentric bottom-mounted cylinder system has been investigated using the eigenfunction expansion approach. This system contains an outer porous cylinder and an inner impermeable cylinder, which are connected by dual porous ring plates. Both cylinders are surface-piercing and rigidly installed on the flat bottom of the ocean, while the porous ring plates are fixed below the free water surface. The analytical solution of the velocity potentials can be obtained by matching the boundary conditions. After obtaining the velocity potentials, the wave force and free surface elevation are computed. The numerical results obtained for limiting cases agreed well with the published results. The results of the study show that reducing the draft, spacing, and permeability of the dual plates all contribute to reduce the horizontal force of the inner cylinder. However, the significance of the lower plate is mainly to cope with the condition where the water surface is lower than the upper plate.

1. Introduction

The supporting members of offshore structures are usually isolated cylinders or cylindrical arrays, which often bear huge hydrodynamic forces. Porous structures can reduce the wave action and optimize the hydrodynamic performance of impermeable structures, so they are considered to have application prospects. Many scholars have studied this kind of combination structures.

Wang and Ren (1994) was the first to investigate the wave interaction with a bottom-mounted concentric cylinder system theoretically in which the outer cylinder is porous and the inner cylinder is impermeable. Their results show that compared with the cylinder directly subjected to wave impact, the existence of the outer porous cylinder not only reduces the hydrodynamic force acting on the inner cylinder but also reduces the wave amplitude on the windward side of the inner cylinder. Almost at the same time, Darwiche et al. (1994) segmented the boundary conditions and studied a bottom-mounted concentric cylinder system with a semi porous outer cylinder. The so-called semi porous outer cylinder means that the outer cylinder is porous in the vicinity of the free water surface and impermeable at a certain distance below the free water surface. On the foundation of Darwiche et al. (1994)'s research, Williams and Li (1998) investigated a semi-porous concentric cylinder system mounted on a storage tank. Li et al. (2003) studied a concentric cylinder system with a semi porous outer cylinder, which is another extension to the model studied by Darwiche et al. (1994). The outer cylinder of the model is porous in a certain angle range, while the rest is impermeable. Vijayalakshmi et al. (2007) and Vijayalakshmi et al. (2008) studied the interaction between waves and two concentric cylinders by experimental and numerical methods. Mandal et al. (2013) and Mandal and Sahoo (2015) investigated the hydroelastic analysis of a concentric cylinder system with a flexible outer wall in a single-layer fluid and a two-layer fluid. Liu et al. (2018) studied the interaction of waves with a concentric cylinder system with multiple outer porous cylinders. Cong and Liu (2020) investigated the mean drift wave force on a concentric cylinder system.

The research mentioned above showed that the hydrodynamic performance of the structure can be improved by setting the porous outer cylinder and reasonably designing the structure parameters. In addition to the structural type of setting the outer cylinder, some scholars found that the porous disk may also be conducive to improving the hydrodynamic performance of the structure, but the relevant research is

* Corresponding author.
E-mail address: heuguangyuan@126.com (G. Wang).

https://doi.org/10.1016/j.oceaneng.2022.113613
Received 30 September 2022; Received in revised form 12 December 2022; Accepted 31 December 2022
Available online 11 January 2023

relatively deficient. Wu and Chwang (2002) analyzed the phenomenon of wave diffraction by a vertical cylinder with a submerged horizontal porous ring plate. They found that the presence of the plate helped to reduce the horizontal force of the cylinder. Recently, Wang et al. (2021) investigated the wave diffraction from a concentric truncated cylinder system with a porous ring plate fixed inside. The research show that the closer the ring plate is to the still water surface, the smaller the horizontal force and overturning moment of the structure. This is due to the fact that the ocean wave energy is concentrated on the water surface, so the closer the disk is to the still water surface, the higher its wave dissipation efficiency. The position of the still water surface in the ocean varies greatly by the tides. Therefore, it has been suggested to use dual plates as a wave dissipation structure to improve its efficiency. Studies on dual plates have mostly focused on their performance as breakwaters (Cheong and Patarapanich, 1992; Wang and Shen, 1999; Wang et al., 2006; Neelamani and Gayathri, 2006; Liu et al., 2008; Cho et al., 2013; Liu and Li, 2014), while no scholars have considered their effects on the hydrodynamic performance of concentric cylinder system.

In this paper, a concentric bottom-mounted cylinder system with dual porous ring plates is studied. The concentric cylinder system consists of a porous outer cylinder and an impermeable inner cylinder, which are rigidly connected by dual porous ring plates below the still water surface. Both cylinders are surface-piercing and rigidly installed on the flat bottom of the ocean. The dual plates can cope with tide-induced water level changes, ensure that the structure still has a certain energy dissipation capacity after the still water level is lower than the upper plate. The hydrodynamic forces of the inner and outer cylinders under the action of linear waves are calculated by the method of eigenfunction expansion and boundary conditions matching. This paper studies the effects of the wave and structure parameters, which has guiding significance for the engineering application of the structure.

The mathematical model of this study is showed in Section 2. The analytic solution of diffraction is derived in Section 3. The calculation program based on the theory is verified in Section 4. Some cases are given in Section 5. The last section is the conclusion of this paper.

2. Mathematical model

The model of wave interaction with a concentric cylinder system with dual porous ring plates fixed inside is shown in Fig. 1. A cylindrical coordinate system and a Cartesian coordinate system are established at the intersection of the center of the cylinder system and the still water surface, and the z-axis is vertical upward. The seabed is considered to be flat and impermeable, and the symbol h denotes the depth of water. The draft of the dual porous ring plates is d_1 and d_2 respectively. Symbols a_1 and a_2 represent the radii of the inner impermeable cylinder and the outer porous cylinder respectively. The fluid is divided into two regions: the exterior region defined by $\Omega_1 \ \ (a_2 < r,\ 0 \le \theta \le 2\pi,\ -h \le z \le 0)$; the interior region defined by $\Omega_2 \ \ (a_1 < r \le a_2,\ 0 \le \theta \le 2\pi,\ -h \le z \le 0)$.

We assume that the fluid is inviscid and incompressible and that the fluid motion is irrotational. Then we can use a time-dependent velocity potential $\boldsymbol{\Phi}$ to describe the fluid motion. By further considering linear harmonic waves, the velocity potential can be written as

$$\boldsymbol{\Phi}(r,\theta,z,t) = \ \mathrm{Re}\left[\phi(r,\theta,z)\, e^{-\mathrm{i}\omega t}\right], \tag{1}$$

where Re denotes the real part of the argument, $\phi(r,\theta,z)$ the spatial velocity potential, $\mathrm{i} = \sqrt{-1}$, ω the angular frequency and t the time. Now we only need to consider the spatial velocity potential $\phi(r,\theta,z)$. The spatial velocity potential satisfies the Laplace equation:

$$\nabla^2 \phi_j = 0,\ j = 1,\ 2, \tag{2}$$

where the subscript j represents variables with respect to region j.

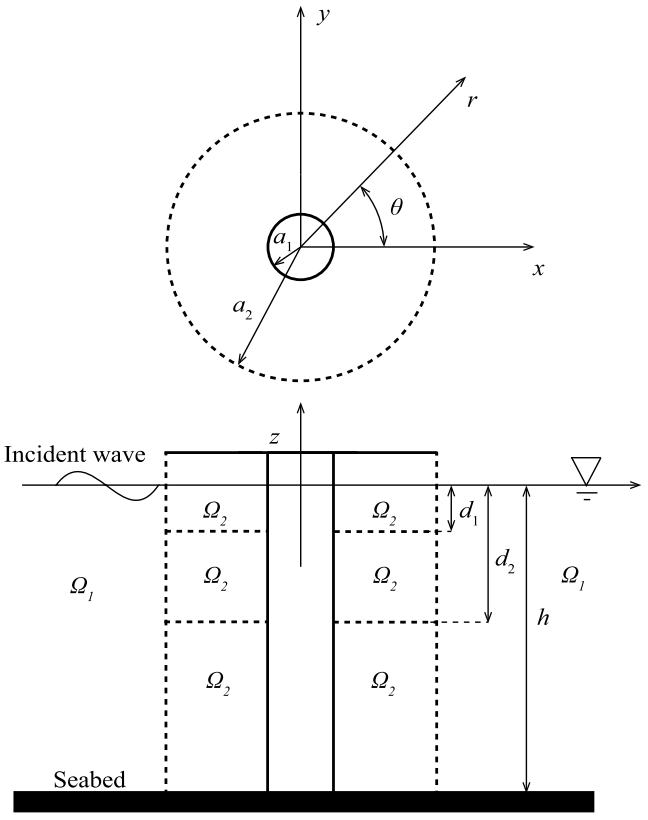

Fig. 1. Schematic diagram of a concentric cylinder system with dual porous ring plates fixed inside.

The velocity potentials in relevant regions also satisfy the impermeable seabed condition, the linear free surface condition, and the far field radiation condition:

$$\frac{\partial \phi_j}{\partial z} = 0,\ z = -h, \quad j = 1,\ 2, \tag{3}$$

$$\frac{\partial \phi_j}{\partial z} = \nu \phi_j,\ z = 0, \quad j = 1,\ 2, \tag{4}$$

$$\lim_{r \longrightarrow \infty} \sqrt{r}\left(\frac{\partial}{\partial r} - \mathrm{i}k_0\right)(\phi_1 - \phi_I) = 0, \tag{5}$$

where $\nu = \omega^2/g$ and g is the acceleration of gravity. k_0 is the incident wavenumber. ϕ_I is the incident velocity potential.

The boundary condition on the impermeable surface of the inner cylinder can be expressed as

$$\frac{\partial \phi_2}{\partial r} = 0, \quad r = a_1,\ -h \le z \le 0. \tag{6}$$

The boundary condition of the porous ring plates and the outer cylinder can be written as follows, respectively:

$$\frac{\partial \phi_2}{\partial z}\Big|_{z=-d_q^+} = \frac{\partial \phi_2}{\partial z}\Big|_{z=-d_q^-} = \frac{\mathrm{i}}{\sigma_q}\left[\phi_2\left(r,\theta,-d_q^-\right) - \phi_2\left(r,\theta,-d_q^+\right)\right], \quad a_1 \le r \le a_2,\ q = 1,\ 2, \tag{7}$$

$$\frac{\partial \phi_2}{\partial r}\Big|_{r=a_2^+} = \frac{\partial \phi_1}{\partial r}\Big|_{r=a_2^-} = \frac{\mathrm{i}}{\sigma_3}\left[\phi_2\left(a_2^-,\ \theta,\ z\right) - \phi_1\left(a_2^+,\ \theta,\ z\right)\right],\ -h \le z \le 0, \tag{8}$$

where $\sigma_q = \mu/\left(\rho l_q \omega\right)\ (q = 1,\ 2,\ 3)$ represent the porous effect parameter of the dual ring plates and the outer cylinder, ρ and μ the water density and dynamic viscosity, l_q the porosity coefficient with a dimension of length. $\sigma_q = 0$ means that the surface is completely

permeable, as if it does not exist. As the σ_q increases to infinity, the surface becomes completely impermeable. The superscript of plus and minus in (7) represent the upper and lower surfaces of the ring plates, respectively. The superscript of plus and minus in (8) represent the outer and inner surfaces of the outer cylinder, respectively.

On the common boundaries between different regions, the velocity potentials must satisfy appropriate transmission condition:

$$\frac{\partial \phi_1}{\partial r} = \frac{\partial \phi_2}{\partial r},\ -h \le z \le 0,\ r = a_2, \tag{9}$$

$$\phi_1 = \phi_2 + \mathrm{i}\sigma_3 \frac{\partial \phi_2}{\partial r},\ -h \le z \le 0,\ r = a_2. \tag{10}$$

3. Analytical solution

The analytic solution of the diffraction problem is obtained by utilizing the method of separating variables in each region. In region Ω_1, the potential ϕ_1 can be written in terms of the following eigenfunction expansion:

$$\phi_1 = -\frac{\mathrm{i}gA}{\omega} \sum_{n=0}^{\infty} \varepsilon_n \cos(n\theta) \left\{ \left[\mathrm{i}^n J_n(k_0 r) + A_{n0} R_n(k_0 r)\right] Z_0(k_0 z) + \sum_{m=1}^{\infty} A_{nm} R_n(k_m r) Z_m(k_m z) \right\}, \tag{11}$$

where the eigenfunctions are defined as

$$R_n(k_m r) = \begin{cases} \frac{H_n(k_m r)}{H_n(k_m a_2)}, & m = 0 \\ \frac{K_n(k_m r)}{K_n(k_m a_2)}, & m \ge 1 \end{cases},$$

$$Z_m(k_m z) = \begin{cases} \frac{\cosh[k_m(z+h)]}{\cosh(k_m h)}, & m = 0 \\ \frac{\cos[k_m(z+h)]}{\cos(k_m h)}, & m \ge 1 \end{cases},$$

and

$$\varepsilon_n = \begin{cases} 1, & n = 0 \\ 0, & n \ge 1 \end{cases}.$$

Here, A is the amplitude of the incident wave, A_{nm} $(n,\ m = 0,\ 1,\ 2, \ldots)$ are unknown coefficients, J_n and H_n denote the first kind of Bessel and Hankel function of order n, while K_n is the second kind of modified Bessel function of order n. Wavenumber k_0 and k_m are the roots of the following dispersion relations:

$$\omega^2 = \begin{cases} gk_m \tanh(k_m h), & m = 0 \\ -gk_m \tan(k_m h), & m \ge 1 \end{cases}.$$

The velocity potential ϕ_2 in the region Ω_2, satisfying the body boundary conditions (3), (4), (6) and the first equal of (7), can be expressed as

$$\phi_2 = -\frac{\mathrm{i}gA}{\omega} \sum_{n=0}^{\infty} \varepsilon_n \cos(n\theta) \sum_{l=1}^{\infty} B_{nl} U_n(\kappa_l r) f(\kappa_l z), \tag{12}$$

where the radial eigenfunction $U_n(\kappa_l r)$ and vertical eigenfunction $f(\kappa_l z)$ are given as:

$$U_n(\kappa_l r) = \frac{H_n'(\kappa_l a_1) J_n(\kappa_l r) - J_n'(\kappa_l a_1) H_n(\kappa_l r)}{H_n'(\kappa_l a_1) J_n(\kappa_l a_2) - J_n'(\kappa_l a_1) H_n(\kappa_l a_2)},$$

$$f(\kappa_l z) = \frac{-\mathrm{i}gA}{\omega} \begin{cases} E_l \sinh[\kappa_l(h-d_2)] \\ \quad \times (\kappa_l \cosh \kappa_l z + \upsilon \sinh \kappa_l z), & -d_1 < z < 0 \\ \{E_l(\kappa_l \cosh \kappa_l z + \upsilon \sinh \kappa_l z) + Q_l \cosh[\kappa_l(z+d_1)]\} \\ \quad \times \sinh[\kappa_l(h-d_2)], & -d_2 < z < -d_1 \\ \{E_l D(\kappa_l d_2) - Q_l \sinh[\kappa_l(d_2-d_1)]\} \\ \quad \times \cosh[\kappa_l(z+h)], & -h < z < -d_2, \end{cases}$$

Here, B_{nl} $(n = 0,\ 1,\ 2, \ldots;\ l = 1,\ 2,\ 3, \ldots)$ are unknown coefficients, the prime denotes the first derivative with respect to the argument. The symbol $D(\kappa_l z)$ is defined as $D(\kappa_l z) = \upsilon \cosh(\kappa_l z) - \kappa_l \sinh(\kappa_l z)$. E_l and Q_l are unknown coefficients that can be determined by substituting Eq. (12) into the second equal of Eq. (7):

$$\mathrm{i}\sigma_1 E_l \kappa_l D(\kappa_l d_1) + Q_l = 0, \tag{13}$$

$$\mathrm{i}\sigma_2 \kappa_l \sinh[\kappa_l(h-d_2)] \{E_l D(\kappa_l d_2) - Q_l \sinh[\kappa_l(d_2-d_1)]\} + E_l D(\kappa_l h) - Q_l \sinh[\kappa_l(h-d_1)] = 0. \tag{14}$$

The above linear equations are homogeneous. To satisfy that the solutions of the coefficients E_l and Q_l are nontrivial, the determinant of the linear system should be equal to 0. Thus the following "dispersion–dissipation relation" is obtained:

$$D(\kappa_l h) + \mathrm{i}\sigma_2 \kappa_l D(\kappa_l d_2) \sinh[\kappa_l(h-d_2)] + \mathrm{i}\sigma_1 \kappa_l D(\kappa_l d_1) \sinh[\kappa_l(h-d_1)] = \sigma_1 \sigma_2 \kappa_l^2 D(\kappa_l d_1) \sinh[\kappa_l(h-d_2)] \sinh[\kappa_l(d_2-d_1)].$$

Bao et al. (2009) gives an iterative method to solve the above complex eigenvalues κ_l.

Application of the transmission condition (9)–(10), two sets of algebraic equations can be derived by using the orthogonal properties of the vertical eigenfunctions in each fluid region:

$$\mathrm{i}^n k_0 J_n'(k_0 a_2) \int_{-h}^{0} Z_0(k_0 z) f(\kappa_l z)\, dz + \sum_{m=0}^{\infty} A_{nm} R_n'(k_m a_2) \int_{-h}^{0} Z_m(k_m z) f(\kappa_l z)\, dz = B_{nl} U_n'(\kappa_l a_2) \int_{-h}^{0} [f_l(\kappa_l z)]^2 dz, \tag{15}$$

$$\mathrm{i}^n J_n(k_0 a_2) \int_{-h}^{0} Z_0(k_0 z) f(\kappa_l z)\, dz + \sum_{m=0}^{\infty} A_{nm} \int_{-h}^{0} Z_m(k_m z) f(\kappa_l z)\, dz = B_{nl} [1 + \mathrm{i}\sigma_3 U_n'(\kappa_l a_2)] \int_{-h}^{0} [f_l(\kappa_l z)]^2 dz. \tag{16}$$

Solving the Eqs. (15)–(16), the coefficients A_{mn} and B_{nl} can be obtained. Then the velocity potential in each region can be determined. Finally, the hydrodynamic forces and the free surface elevations can be calculated by the velocity potential.

The horizontal force on the inner cylinder F_I and outer cylinder F_O in the direction of wave can be obtained by integrating the pressure difference between two sides of the wetted body surface at $r = a_1$ and $r = a_2$, respectively:

$$F_I = \mathrm{i}\omega\rho a_1 \int_0^{2\pi} \int_{-h}^{0} \phi_2(a_1, \theta, z) \cdot (-\cos\theta)\, d\theta dz, \tag{17}$$

$$F_O = \mathrm{i}\omega\rho a_2 \int_0^{2\pi} \int_{-h}^{0} [\phi_1(a_2, \theta, z) - \phi_2(a_2, \theta, z)] \cdot (-\cos\theta)\, d\theta dz. \tag{18}$$

Similarly, the vertical force F_H can be given as:

$$F_H = F_H^U + F_H^L = \rho\omega \int_0^{2\pi} d\theta \int_{a_1}^{a_2} \left[\sigma_1 \frac{\partial \phi_2(r, \theta, -d_1)}{\partial z} + \sigma_2 \frac{\partial \phi_2(r, \theta, -d_2)}{\partial z}\right] r dr. \tag{19}$$

where F_H^U and F_H^L represent the heave force of the upper and lower plates respectively.

The overturning moment F_P of the system can be calculated by

$$F_p = \mathrm{i}\rho\omega a_1 \int_{-h}^{0} \int_0^{2\pi} \phi_2(z+h)(-\cos\theta)\, d\theta dz + \mathrm{i}\rho\omega a_2 \int_{-h}^{0} \int_0^{2\pi} (\phi_1 - \phi_2)(z+h)(-\cos\theta)\, d\theta dz$$

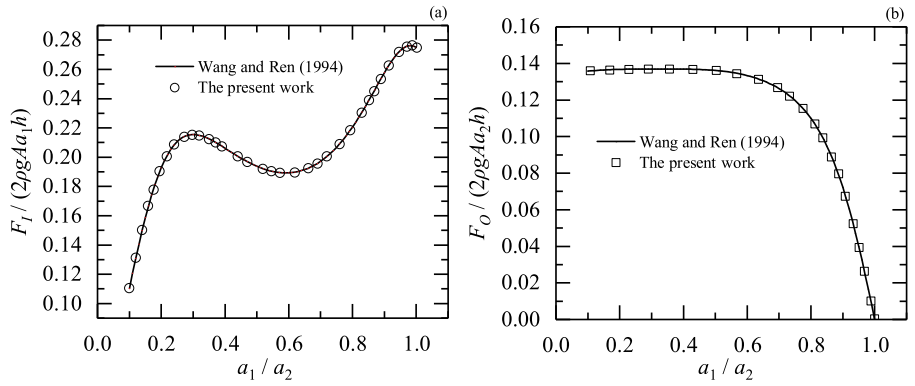

Fig. 2. Comparison between the present model and that of Wang and Ren (1994), where $h = 15$ m, $a_2 = 10$ m, $b_1 = b_2 = 1000\pi$, $b_3 = 2\pi$, $k_0 = 0.3334$, $d_1 = 1$ m, $d_2 = 2$ m.

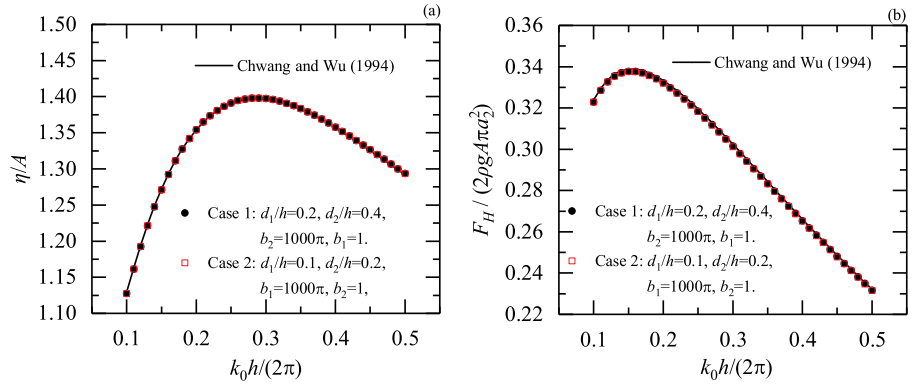

Fig. 3. Comparison between the present model and that of Chwang and Wu (1994), where $k_0 a_2/\pi = 0.4, b_3 = 1000\pi$, and $r = a_2, \theta = 0$ for (a).

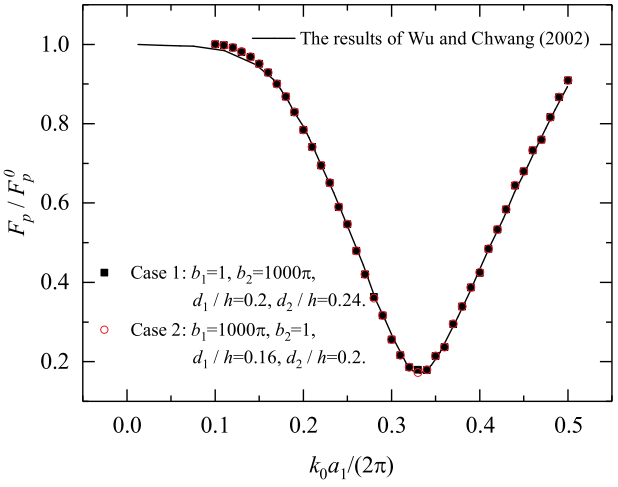

Fig. 4. Comparison between the present model and that of Wu and Chwang (2002), where $k_0 h = \pi, a_1/a_2 = 0.7, b_3 = 1000\pi$.

$$+ \rho\omega \int_{a_1}^{a_2} \int_0^{2\pi} \sigma_1 \frac{\partial \phi_2}{\partial z} |_{z=-d_1} \left(-r^2 \cos\theta\right) d\theta dr$$
$$+ \rho\omega \int_{a_1}^{a_2} \int_0^{2\pi} \sigma_2 \frac{\partial \phi_2}{\partial z} |_{z=-d_2} \left(-r^2 \cos\theta\right) d\theta dr. \quad (20)$$

The free surface elevations can also be calculated by the linear Bernoulli equation:

$$\eta(r,\theta,z) = \frac{i\omega}{g} \phi_j(r,\theta,z)|_{z=0}, \quad j = 1,2. \quad (21)$$

4. Validations

In order to verify the analytical solution, a program based on Fortran is developed. $b_q = 2\pi/(k_0\sigma_q)$ $(q = 1, 2, 3)$ are introduced to express the dimensionless porous effect parameter of the ring plates (b_1 for the upper plate and b_2 for the lower plate) and the outer cylinder (b_3), respectively.

To solve for the unknown coefficients of Eqs. (15)–(16), we truncate both l and m to l_0 and n to n_0. First, the convergence test of the analytic solutions with l_0 and n_0 are list in Table 1 for the model $a_1 = 4$ m, $a_2 = 8$ m, $h = 10$ m, $d_1 = 0.5$ m, $d_2 = 1.5$ m, $b_1 = b_2 = b_3 = 2\pi, k_0 a_2 = 1.0$, in which the parameters are defined as

$$f_H = |F_H/\rho g A \pi a_1^2|, \ f_I = |F_I/2\rho g A a_1 h|, \ f_O = |F_O/2\rho g A a_2 h|,$$
$$\gamma_I = |\eta_I(a_1, 0, 0)/(2A)|, \ \gamma_E = |\eta_E(a_2, \pi, 0)/(2A)|.$$

It can be seen that $l_0 = 20$ and $n_0 = 4$ are enough to ensure convergence of the numerical results within three decimal places, as sufficiently accurate for engineering purposes.

When the dimensionless porous effect parameters of the ring plates b_1 and b_2 approaches infinity, the effect of them disappears, and the model degenerates into a concentric cylinder system, which is the same as the model studied by Wang and Ren (1994). The parameters are selected as follows: $h = 15$ m, $a_2 = 10$ m, $b_1 = b_2 = 1000\pi$, $b_3 = 2\pi$, $k_0 = 0.3334$, $d_1 = 1$ m, $d_2 = 2$ m. Fig. 2 shows the comparison between the present model and that of Wang and Ren (1994), in which the horizontal force of the inner and outer cylinder is non-dimensionalized by $2\rho g A a_1 h$ and $2\rho g A a_2 h$, respectively. It can be seen that the present method is reliable in calculating the horizontal force of the inner and outer cylinder, based on comparison with published results of Wang and Ren (1994).

To further verify the vertical force and free surface elevation, we consider the limiting case of reducing the model to a porous disk.

Table 1
Convergence test on the dimensionless wave force and run-up for $a_1 = 4$ m, $a_2 = 8$ m, $h = 10$ m, $d_1 = 0.5$ m, $d_2 = 1.5$ m, $k_0a_2 = 1.0$, $b_1 = b_2 = b_3 = 2\pi$,.

l_0	$n_0 = 2$						$n_0 = 4$						$n_0 = 6$					
	f_H	f_I	f_O	f_P	γ_I	γ_E	f_H	f_I	f_O	f_P	γ_I	γ_E	f_H	f_I	f_O	f_P	γ_I	γ_E
2	1.272	0.665	0.459	2.260	0.162	0.698	1.272	0.665	0.459	2.260	0.161	0.665	1.272	0.665	0.459	2.260	0.161	0.665
5	1.152	0.602	0.443	2.119	0.155	0.698	1.152	0.602	0.443	2.119	0.151	0.665	1.152	0.602	0.443	2.119	0.151	0.665
10	1.028	0.678	0.417	2.038	0.290	0.720	1.028	0.678	0.417	2.038	0.286	0.687	1.028	0.678	0.417	2.038	0.286	0.688
20	1.028	0.678	0.417	2.038	0.289	0.720	1.028	0.678	0.417	2.038	0.286	0.688	1.028	0.678	0.417	2.038	0.286	0.688
30	1.028	0.678	0.417	2.038	0.290	0.720	1.028	0.678	0.417	2.038	0.286	0.688	1.028	0.678	0.417	2.038	0.286	0.688

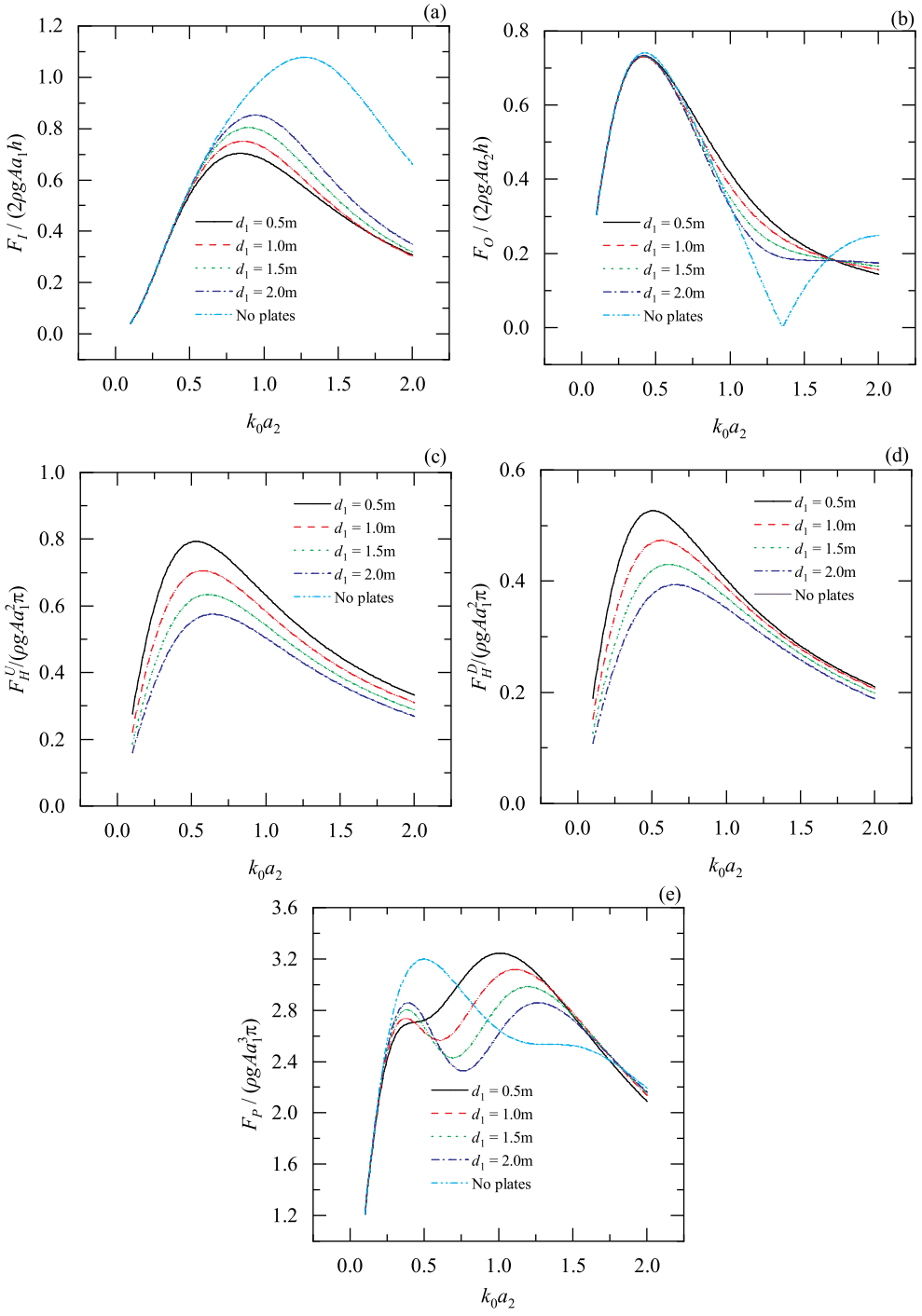

Fig. 5. Variations of the dimensionless hydrodynamic forces vs. wavenumber k_0a_2 for different d_1 at $a_1 = 4$ m, $a_2 = 8$ m, $h = 10$ m, $d_2 - d_1 = 1.0$ m, $b_1 = b_2 = b_3 = 2\pi$: (a) Inner cylinder; (b) Outer cylinder; (c) Upper plate; (d) Lower plate; (e) Overturning moment of system.

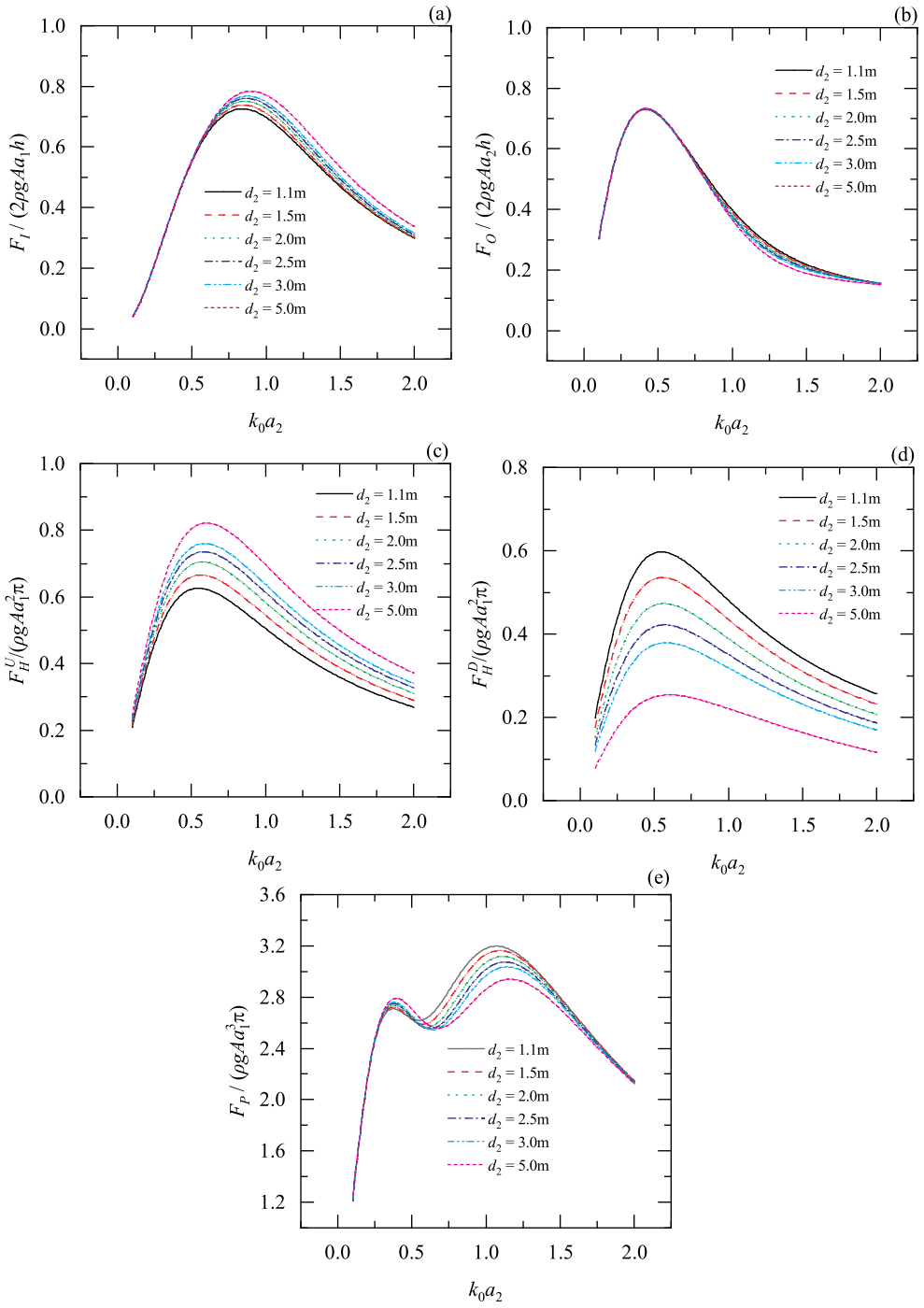

Fig. 6. Variations of the dimensionless hydrodynamic forces vs. wavenumber $k_0 a_2$ for different d_2 at $a_1 = 4$ m, $a_2 = 8$ m, $h = 10$ m, $d_1 = 1.0$ m, $b_1 = b_2 = b_3 = 2\pi$: (a) Inner cylinder; (b) Outer cylinder; (c) Upper plate; (d) Lower plate; (e) Overturning moment of system.

When the dimensionless porous effect of the outer cylinder b_3 approaches to infinity and the radius of the inner cylinder a_1 approaches to infinitesimal, the model degenerates to dual porous disks. Setting the permeability of one of the disks to infinity, the model further degenerates to an isolated disk. The parameters are chosen as $d_1/h = 0.2$, $d_2/h = 0.4$, $k_0 a_2/\pi = 0.4$, $b_2 = b_3 = 1000\pi$, $b_1 = 1$ for case 1, and $d_1/h = 0.1$, $d_2/h = 0.2$, $k_0 a_2/\pi = 0.4$, $b_1 = b_3 = 1000\pi$, $b_2 = 1$ for case 2. Fig. 3 shows the comparison of dimensionless free surface elevation and heave force between the present results and the corresponding solution by Chwang and Wu (1994). The free surface elevation and vertical force are non-dimensionalized by the wave amplitude A and $2\rho g A \pi a_2^2$. This figure shows that the calculation results of the free surface elevation and vertical force are coincide with the results of Chwang and Wu (1994).

To verify the overturning moment, we specify $a_1/a_2 = 0.7$, $k_0 h = \pi$ and $b_3 = 1000\pi$ in the present model. In case 1, the lower plate is completely permeable, i.e. $b_2 = 1000\pi$, and $d_1/h = 0.2$, $d_2/h = 0.24$, $b_1 = 1$. Similarly, the upper plate is completely permeable, i.e. $b_1 = 1000\pi$, and $d_1/h = 0.16$, $d_2/h = 0.2$, $b_2 = 1$ in case 2. As shown in Fig. 4, the numerical results of the two cases agree well with the result of Wu and Chwang (2002), where F_P^0 indicates that all porous surfaces are completely permeable. Fig. 4 can demonstrate the validity of the present formula of overturning moment.

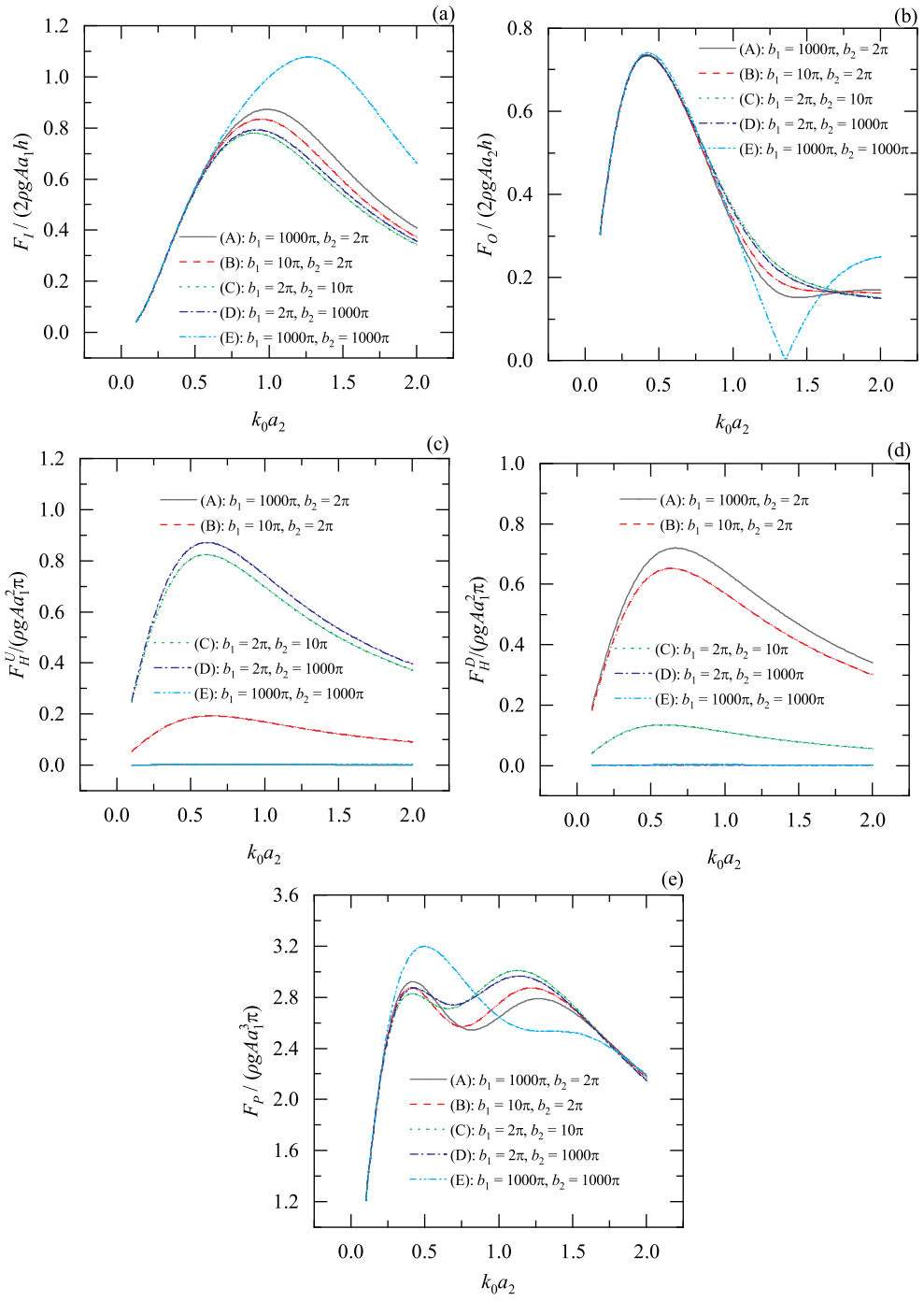

Fig. 7. Variations of the dimensionless hydrodynamic forces vs. wavenumber $k_0 a_2$ for different b_1 and b_2 at $a_1 = 4$ m, $a_2 = 8$ m, $h = 10$ m, $d_1 = 1.0$ m, $d_2 = 2.0$ m, $b_3 = 2\pi$: (a) Inner cylinder; (b) Outer cylinder; (c) Upper plate; (d) Lower plate; (e) Overturning moment of system.

Through the above verification, the present results are proved reliable.

5. The numerical results

5.1. Hydrodynamic forces

5.1.1. Effect of the dual plates draft-depth

Fig. 5 shows the variation of the hydrodynamic forces with the dimensionless wavenumber $k_0 a_2$ for different d_1 at $a_1 = 4$ m, $a_2 = 8$ m, $h = 10$ m, $d_2 - d_1 = 1.0$ m, $b_1 = b_2 = b_3 = 2\pi$. From Fig. 5(a), it can be observed that all curves keep a similar trend, that is, with the increase of the dimensionless wavenumber $k_0 a_2$, the horizontal force of the inner cylinder increases firstly and then gradually decreases. Meanwhile, with the decrease of d_1, the peak value of the horizontal force acting on the inner cylinder decreases gradually, and the wavenumber corresponding to the peak value moves to the left. Compared with the case without dual plates, the peak horizontal force of the inner cylinder is reduced by about 35% for $d_1 = 0.5$ m. It can be seen from Fig. 5(b) that the horizontal force of the outer cylinder is only slightly affected by d_1 in the high frequency region. From Fig. 5(c) and (d), the peak values of the upper and lower plate vertical force increase with the decrease of d_1. The upper plate vertical force is more significant than the lower in the whole frequency range, which is because the wave

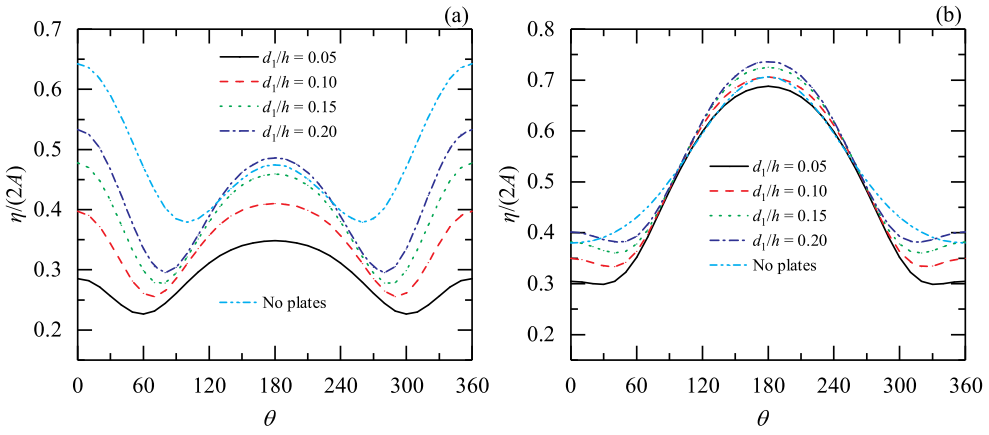

Fig. 8. Variations of the dimensionless wave run up on cylinders for different d_1/h at $a_1 = 4$ m, $a_2 = 8$ m, $h = 10$ m, $d_2 - d_1 = 1.0$ m, $b_1 = b_2 = b_3 = 2\pi$, $k_0 a_2 = 1.0$: (a) Inner cylinder; (b) Outer cylinder.

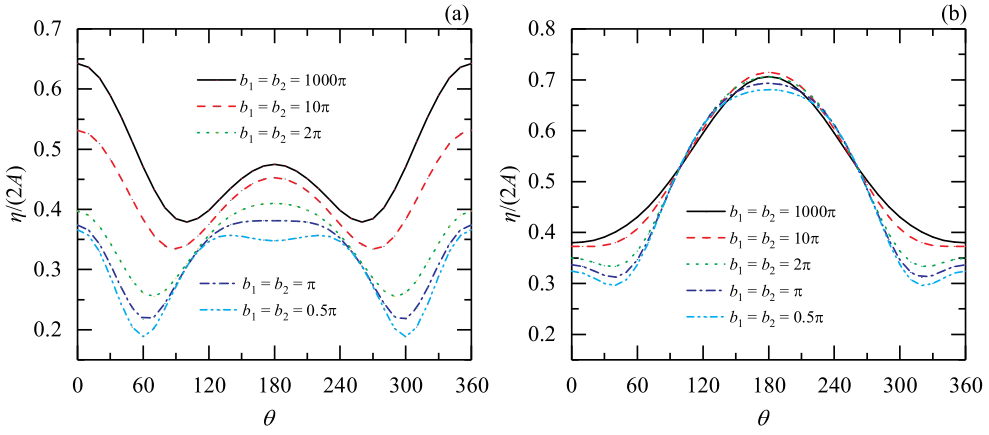

Fig. 9. Variations of the dimensionless wave run up on cylinders for different b_1 and b_2 at $a_1 = 4$ m, $a_2 = 8$ m, $h = 10$ m, $d_2 = 2.0$ m, $d_1 = 1.0$ m, $b_3 = 2\pi$, $k_0 a_2 = 1.0$: (a) Inner cylinder; (b) Outer cylinder.

energy is more dissipated by the upper plate and the exponential decay of wave motion in the vertical direction. According to Fig. 5(e), the overturning moment of system has only one peak point for no plates case. The presence of dual plates leads to a second peak point of curves. The first peak decreases with the decrease of d_1, while the second peak increases with the decrease of d_1.

5.1.2. Effect of the dual plates spacing

The effect of the dual plates spacing on the dimensionless hydrodynamic forces is shown in Fig. 6, in which the curves are plotted for different d_2 at $a_1 = 4$ m, $a_2 = 8$ m, $h = 10$ m, $d_1 = 1.0$ m, $b_1 = b_2 = b_3 = 2\pi$. As can be observed from Fig. 6(a) and (b), when the upper plate is fixed, reducing the spacing between the two plates can slightly reduce the inner cylinder horizontal force, while the outer cylinder has basically no effect. Compared to $d_2 = 5.0$ m, the horizontal force of the inner cylinder is reduced by about 7.7% for the case of $d_2 = 1.1$ m. This shows that when the upper plate is submerged, the lower plate has little effect on the horizontal force of the inner and outer cylinders. The significance of the lower plate is to ensure that the structure still has the ability to dissipate surface waves after the water surface drops below the upper plate. From Fig. 6(c) and (d), it can be shown that decreasing the draft depth of the lower plate will decrease the peak vertical force of the upper plate while increasing the value of the lower plate. This indicates that the closer the lower plate is to the upper plate, the greater its role in the dissipation of wave energy in the system. For the overturning moment of the system, as shown in Fig. 6(e), the first peak decreases and the second peak increases as the draft of the lower plate decreases.

5.1.3. Effect of the dual plates permeability

The influence of the dual plates permeability is shown in Fig. 7, in which the parameters are chosen as: $a_1 = 4$ m, $a_2 = 8$ m, $h = 10$ m, $d_1 = 1.0$ m, $d_2 = 2.0$ m, $b_3 = 2\pi$. Case (A) and (D) indicate that the upper plate or the lower plate does not exist, respectively. Case (B) and (C) indicate that both plates exist, but the permeability of them are different. From Fig. 7(a) and (b), it can be noticed that reducing the permeability of the dual plates can significantly reduce the peak surge force of the inner cylinder, while it has almost no effect on the outer cylinder. When dual plates are present and the upper plate is less permeable (Case C), the peak horizontal force of the inner cylinder is reduced by about 28% compared to the no plates case. As seen in Fig. 7(c) and (d), the lower the permeability of the plate, the higher the vertical force on it. The dual plates have a protective effect on each other. It can be seen from Fig. 7(e) that the first peak of the overturning moment decreases gradually and the second peak increases gradually with the decrease of the permeability of the dual plates.

5.2. Wave elevations at the free surface

5.2.1. Effect of the dual plates draft-depth

Fig. 8 shows the variation of the dimensionless wave run up on the inner and outer cylinder for different d_1/h at $a_1 = 4$ m, $a_2 = 8$ m, $h = 10$ m, $d_2 - d_1 = 1.0$ m, $b_1 = b_2 = b_3 = 2\pi$, $k_0 a_2 = 1.0$. By examining Fig. 7(a), it can be seen that lowering the draft depth of dual plates helps to reduce the wave run up on the inner and outer cylinders. This indicates that the smaller the draft depth of the dual plates, the greater their ability to dissipate wave energy.

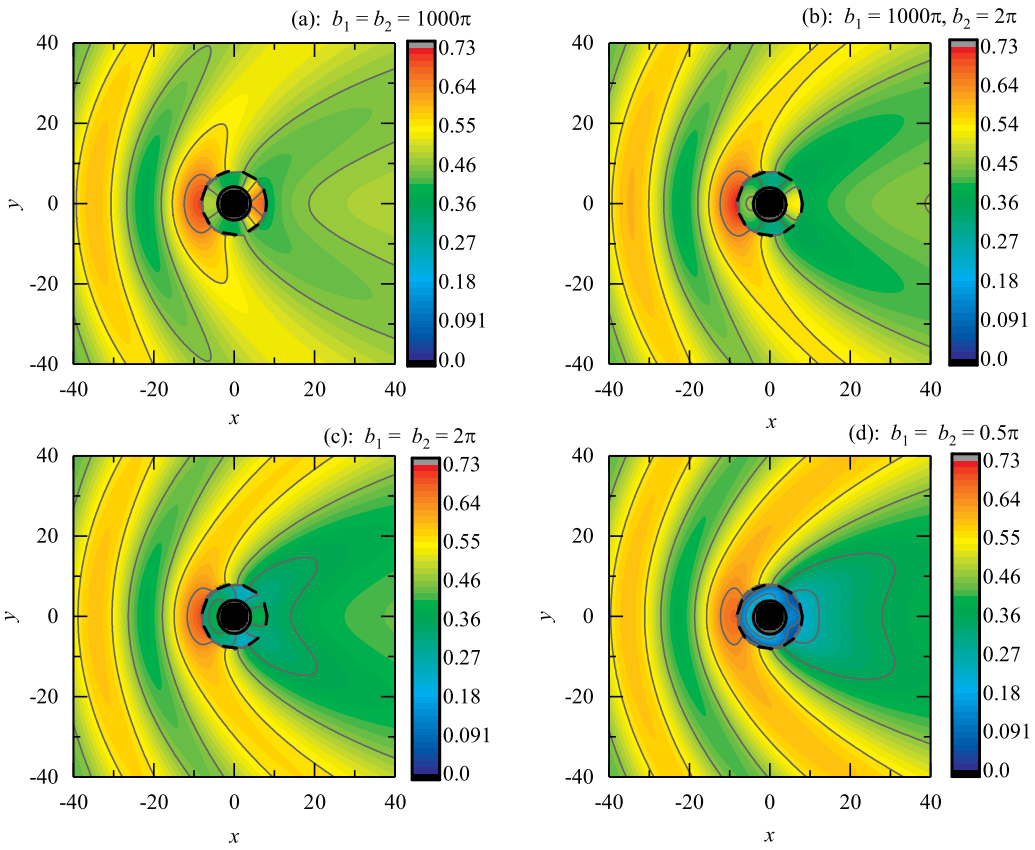

Fig. 10. Comparison of free surface elevation for $a_1 = 4$ m, $a_2 = 8$ m, $h = 10$ m, $d_1 = 0.5$ m, $d_2 = 1.5$ m, $b_3 = 2\pi$, $k_0 a_2 = 1.0$: (a) $b_1 = b_2 = 1000\pi$; (b) $b_1 = 1000\pi$, $b_2 = 2\pi$; (c) $b_1 = b_2 = 2\pi$; (d) $b_1 = b_2 = 0.5\pi$.

5.2.2. *Effect of the dual plates permeability*

Fig. 9 shows the variation of the dimensionless wave run up on the inner and outer cylinder for different b_1 and b_2 at $a_1 = 4$ m, $a_2 = 8$ m, $h = 10$ m, $d_1 = 1.0$ m, $d_2 = 2.0$ m, $b_3 = 2\pi$, $k_0 a_2 = 1.0$. As can be seen from Fig. 9, reducing the permeability of the dual plates helps to reduce the wave run up on the inner and outer cylinders. This suggests that the smaller the permeability of the dual plates, the greater their ability to dissipate wave energy.

The influence of the permeability of the upper and lower ring plates on the fluid region can also be revealed by calculating the wave elevations at the free surface. Fig. 10 shows the dimensionless wave elevations at the free surface $\eta/(2A)$ in the vicinity of the system, which the parameters are chosen as $a_1 = 4$ m, $a_2 = 8$ m, $h = 10$ m, $d_1 = 0.5$ m, $d_2 = 1.5$ m, $b_3 = 2\pi$, $k_0 a_2 = 1.0$. The following four groups of parameters are selected: (a) both of dual plates are completely porous ($b_1 = b_2 = 1000\pi$), and the model is equivalent to a concentric cylinder system; (b) the upper plate is completely porous ($b_1 = 1000\pi$) and the lower plate is porous ($b_2 = 2\pi$); (c) the dual plates are porous ($b_1 = b_2 = 2\pi$); (d) the dual plates are porous ($b_1 = b_2 = 0.5\pi$). Comparing with Fig. 10(b) and (a), it can be seen that the existence of a single porous plate significantly alleviates the wave oscillation in the annular region, mainly in the form of reduced free surface elevation on the downstream side. From the comparison of Fig. 10(c) and (b), it can be observed that the addition of another plate failed to significantly reduce the free surface elevation in the annular region. At this point, the lower plate is more meaningful to cope with the tide-induced water depth variation. From Fig. 10(d) and (c), it can be concluded that reducing dual plates permeability could further reduce the free surface elevation in the annular region. Fig. 10(a)–(d) show that in the case of the upper plate submerged, it is more effective to reduce the permeability of the plate than to add a plate in order to increase the wave dissipation. And if the variation of water depth is considered, dual plates are obviously more advantageous.

6. Conclusions

Based on the linear potential wave theory, the hydrodynamic performance of a concentric bottom-mounted cylinder system with dual porous ring plates is studied. The velocity potential of each region is obtained by the method of eigenfunction expansion and boundary conditions matching. The hydrodynamic forces are obtained by integrating the pressure difference between two sides of the wetted body surface. The calculation results are compared with published papers. This paper analyzes the draft, spacing, and permeability of the dual plates on the effect of the diffraction process.

The results show that reducing the dual plates draft, spacing, and permeability can increase the wave dissipation, which is manifested by the simultaneous reduction of the horizontal force on the inner cylinder and the free surface elevation in the annular region. However, all these measures have little effect on the horizontal force of the outer cylinder. In addition, the results of the study also show that the lower plate provides limited improvement in wave dissipation capacity of the structure. The significance of it is mainly to ensure that the structure still has a certain ability to dissipate surface wave energy after the water depth change causes the upper plate above the water surface.

In this paper, Darcy's law is used to analyze the interaction between waves and porous plates. However, it is considered as an inadequate description of the pressure drop condition when the plate opening is large. The quadratic pressure drop model offers a more reasonable alternative that also directly considers the effect of wave height on wave energy dissipation. Related work will be carried out in the future.

CRediT authorship contribution statement

MoHan Zhang: Conceptualization, Methodology. **Xiang Wang:** Methodology, Writing - Revise draft. **GuangYuan Wang:** Software,

Data curation, Writing - Original draft. **Jin Wang:** Validation, Writing – review & editing. **PengYuan Zhao:** Writing – review & editing.

Declaration of competing interest

The authors declare that they have no known competing financial interests or personal relationships that could have appeared to influence the work reported in this paper.

Data availability

The authors are unable or have chosen not to specify which data has been used.

Acknowledgment

The authors would like to express their gratitude for the financial support of the Scientific Research Innovation Fund Project of Tianjin Water Transport Engineering Survey and Design Institute Co., Ltd (Grant no. SJY202110).

References

Bao, W., Kinoshita, T., Zhao, F., 2009. Wave forces acting on a semi-submerged porous circular cylinder. Proc. Inst. Mech. Eng. M 223 (3), 349–360.

Cheong, H.-F., Patarapanich, M., 1992. Reflection and transmission of random waves by a horizontal double-plate breakwater. Coast. Eng. 18 (1–2), 63–82. http://dx.doi.org/10.1016/0378-3839(92)90005-F.

Cho, I., Koh, H., Kim, J., Kim, M., 2013. Wave scattering by dual submerged horizontal porous plates. Ocean Eng. 73, 149–158. http://dx.doi.org/10.1016/j.oceaneng.2013.08.008.

Chwang, A.T., Wu, J., 1994. Wave scattering by submerged porous disk. J. Eng. Mech. 120 (12), 2575–2587.

Cong, P., Liu, Y., 2020. Local Enhancements of the mean drift wave force on a vertical column shielded by an exterior thin porous shell. J. Mar. Sci. Eng. 8 (5), 349.

Darwiche, M., Williams, A., Wang, K.-H., 1994. Wave interaction with semiporous cylindrical breakwater. J. Waterw. Port Coast. Ocean Eng. 120 (4), 382–403.

Li, Y., Sun, L., Teng, B., 2003. Wave action on double-cylinder structure with perforated outer wall. In: International Conference on Offshore Mechanics and Arctic Engineering, Vol. 36819. pp. 149–156.

Liu, Y., Li, H.-j., 2014. Wave scattering by dual submerged horizontal porous plates: Further results. Ocean Eng. 81, 158–163. http://dx.doi.org/10.1016/j.oceaneng.2014.02.004.

Liu, Y., Li, Y.-c., Teng, B., Dong, S., 2008. Wave motion over a submerged breakwater with an upper horizontal porous plate and a lower horizontal solid plate. Ocean Eng. 35 (16), 1588–1596.

Liu, H., Zhang, L., Chen, H., Zhang, W., Liu, M., 2018. Wave diffraction by vertical cylinder with multiple concentric perforated walls. Ocean Eng. 166, 242–252.

Mandal, S., Datta, N., Sahoo, T., 2013. Hydroelastic analysis of surface wave interaction with concentric porous and flexible cylinder systems. J. Fluids Struct. 42, 437–455.

Mandal, S., Sahoo, T., 2015. Axisymmetric gravity wave diffraction by flexible porous cylinder system in two-layer fluid. Ocean Eng. 106, 87–101.

Neelamani, S., Gayathri, T., 2006. Wave interaction with twin plate wave barrier. Ocean Eng. 33 (3–4), 495–516. http://dx.doi.org/10.1016/j.oceaneng.2005.03.009.

Vijayalakshmi, K., Neelamani, S., Sundaravadivelu, R., Murali, K., 2007. Wave runup on a concentric twin perforated circular cylinder. Ocean Eng. 34 (2), 327–336.

Vijayalakshmi, K., Sundaravadivelu, R., Murali, K., Neelamani, S., 2008. Hydrodynamics of a concentric twin perforated circular cylinder system. J. Waterw. Port Coast. Ocean Eng. 134 (3), 166–177.

Wang, K.-H., Ren, X., 1994. Wave interaction with a concentric porous cylinder system. Ocean Eng. 21 (4), 343–360.

Wang, K.-H., Shen, Q., 1999. Wave motion over a group of submerged horizontal plates. Internat. J. Engrg. Sci. 37 (6), 703–715. http://dx.doi.org/10.1016/S0020-7225(98)00094-9.

Wang, Y., Wang, G., Li, G., 2006. Experimental study on the performance of the multiple-layer breakwater. Ocean Eng. 33 (13), 1829–1839. http://dx.doi.org/10.1016/j.oceaneng.2005.10.017.

Wang, G., Yu, F., Zhang, H., Zhang, E., Li, Z., 2021. Wave diffraction from a concentric truncated cylinder system with a porous ring plate fixed inside. Ocean Eng. 228, 108932.

Williams, A., Li, W., 1998. Wave interaction with a semi-porous cylindrical breakwater mounted on a storage tank. Ocean Eng. 25 (2–3), 195–219.

Wu, J., Chwang, A.T., 2002. Wave diffraction by a vertical cylinder with a porous ring plate. J. Eng. Mech. 128 (2), 164–171.